



HAL
open science

Kinetics of Interaction between ADP-ribosylation Factor-1 (Arf1) and the Sec7 Domain of Arno Guanine Nucleotide Exchange Factor, Modulation by Allosteric Factors, and the Uncompetitive Inhibitor Brefeldin A.

Jad Rouhana, Andre Padilla, Sebastien Estaran, Sana Bakari, Stephane Delbecq, Yvan Boublik, Joel Chopineau, Martine Pugnieri, Alain Chavanieu

► To cite this version:

Jad Rouhana, Andre Padilla, Sebastien Estaran, Sana Bakari, Stephane Delbecq, et al.. Kinetics of Interaction between ADP-ribosylation Factor-1 (Arf1) and the Sec7 Domain of Arno Guanine Nucleotide Exchange Factor, Modulation by Allosteric Factors, and the Uncompetitive Inhibitor Brefeldin A.: Allosteric and uncompetitive modulations of Arf1-Arno interaction. *Journal of Biological Chemistry*, 2013, 288 (7), pp.4659-72. 10.1074/jbc.M112.391748 . inserm-00773549

HAL Id: inserm-00773549

<https://inserm.hal.science/inserm-00773549>

Submitted on 30 Nov 2013

HAL is a multi-disciplinary open access archive for the deposit and dissemination of scientific research documents, whether they are published or not. The documents may come from teaching and research institutions in France or abroad, or from public or private research centers.

L'archive ouverte pluridisciplinaire **HAL**, est destinée au dépôt et à la diffusion de documents scientifiques de niveau recherche, publiés ou non, émanant des établissements d'enseignement et de recherche français ou étrangers, des laboratoires publics ou privés.

Kinetics of Interaction between ADP-ribosylation Factor-1 (Arf1) and Sec7 Domain of Arno
Guanine Nucleotide Exchange Factor, Modulation by allosteric factors and the uncompetitive
inhibitor Brefeldin A [§]

**Jad Rouhana¹, André Padilla³, Sébastien Estaran¹, Sana Bakari¹, Stephan Delbecq⁵, Yvan
Boublik⁴, Joel Chopineau⁶⁻⁷, Martine Pugnère^{2*} and Alain Chavanieu^{1*+}**

¹From the Institut des Biomolécules Max Mousseron (IBMM) UMR 5247 CNRS-Universités Montpellier 1 et 2 Faculté de Pharmacie, 15 avenue Charles Flahault BP14491 34093 Montpellier cedex 5, France. ²IRCM, Institut de Recherche en Cancérologie de Montpellier; INSERM, U896; Université Montpellier 1; CRLC Val d'Aurelle Paul Lamarque Montpellier F-34298, France. ³Centre de Biochimie Structurale, INSERM U554, UMR 5048 CNRS and University Montpellier 1 and 2, 29, rue de Navacelles, 34090 Montpellier, France. ⁴Centre de Recherche de Biochimie Macromoléculaire, CNRS UMR 5237, Universités Montpellier 2 et 1, Montpellier, France; ⁵EA 4558 "Vaccination antiparasitaire", Université Montpellier I, Laboratoire de Biologie Cellulaire et Moléculaire, Faculté de Pharmacie, Montpellier, France. ⁶Institut Charles Gerhardt Montpellier, UMR 5253 CNRS-ENSCM UM2-UM1, Montpellier, France. ⁷ Université de Nîmes, Nîmes, France.

[§] Running title: Allosteric and uncompetitive modulations of Arf1-Arno interaction

To whom correspondence should be addressed. Alain Chavanieu, Institut des Biomolécules Max Mousseron, UMR 5247 CNRS-Universités Montpellier 1 et 2 Faculté de Pharmacie, 15 avenue Charles Flahault BP14491 34093 Montpellier cedex 5, France Phone : 33 (0)4 11 75 95 27 ; Fax: 33 (0). Email : alain.chavanieu@univ-montpl1.fr

*M.P. and A.C. have equally participated to this work

Keywords: • Small gtpases • Guanine nucleotide exchange factor (GEF)
• Allosteric regulation • Brefeldin A (BFA) • Kinetics • Surface plasmon resonance (SPR)

DWC: [Include Document word count here <50,000] = 10538

Background: Kinetic modulations of Arf1-Sec7 domain complex, by the uncompetitive inhibitor BrefeldinA and allosteric factors, are not established.

Results: BrefeldinA reorients the binary Arf1-Sec7 domain complex to an abortive one with reduced association and dissociation rates.

Conclusion: Kinetic hallmarks allow distinguishing the level, nature and fate of interacting species.

Significance: Similar approach will solve the inhibitory mechanism of new inhibitor families of sec7 domains.

Summary

The GDP/GTP nucleotide exchange of Arf1 is catalyzed by Nucleotide Exchange Factors (GEF), such as Arno, which act through their catalytic Sec7 domain. This exchange is a complex mechanism that undergoes conformational changes and intermediate complex species involving several allosteric partners such as nucleotides, Mg^{2+} and Sec7 domains. Using a Surface Plasmon Resonance approach, we characterized the kinetic binding parameters for various intermediate complexes. We first confirmed that both GDP and GTP counteract equivalently to the free-nucleotide binary Arf1/Arno complex stability and revealed that Mg^{2+} potentiates by a factor of 2 the allosteric effect of GDP. Then, we explored the uncompetitive inhibitory mechanism of Brefeldin A (BFA) that conducts to an abortive pentameric Arf1- Mg^{2+} -GDP-BFA-Sec7 complex. With BFA, the association rate of the abortive complex is drastically reduced by a factor of 42 and by contrast, the 15-fold decrease of the dissociation rate concurs to stabilize the pentameric complex. These specific kinetic signatures have allowed distinguishing the level, nature as well as the fate in real time of formed complexes according to experimental conditions. Thus, we showed that in the presence of GDP, BFA-resistant Sec7 domain of Arno can also associate to form a pentameric complex which suggests that the uncompetitive inhibition by BFA and the nucleotide allosteric effect combine to stabilize such abortive complex.

Low molecular weight guanine-nucleotide-binding (G) proteins of the Ras superfamily, also known as small GTPases for their GTP hydrolysis activity, are single-subunit proteins activated by diverse extracellular stimuli and implicated in a number of crucial cellular processes including cell proliferation, differentiation, apoptosis, cytoskeletal organization, cell polarity and

vesicular trafficking (1-4). G proteins act as molecular switches and cycle between a GDP-bound inactive and a GTP-bound active conformation that regulate their ability to interact with downstream effectors and regulatory proteins. The activation is a multistep process that requires the release of the bound GDP and the subsequent binding of GTP. G proteins have a slow nucleotide intrinsic dissociation rate which is accelerated upon binding of Guanine Nucleotide Exchange Factors (GEFs) (5,6). The GDP to GTP exchange process involves a transient G protein-GDP-GEF complex, promptly followed by the dissociation of GDP, forming a high-affinity free-GDP G protein-GEF complex. Then, GTP binds with subnanomolar affinity to the nucleotide binding site on the G protein, disrupting the complex between the G protein and the GEF.

Indeed, an allosteric competitive mechanism model explains the kinetics of nucleotide exchange catalyzed by GEFs (7-9) where the G proteins form stable complexes with nucleotides or with GEFs whereas they can also form transient less stable complexes with simultaneously both GEF and nucleotide. Moreover, crystallographic and biological studies revealed that nucleotide-binding on G protein presents a highly conserved coordination of Mg^{2+} within the site, and disrupting the Mg^{2+} coordination (for instance by a GEF) promotes a nucleotide-free state of the G proteins (10). The cation strengthens the nucleotide binding and reduces its dissociation rate, thus weakening binding of the GEF to the G protein (11-13).

The Ras superfamily is divided into five major families: Ras, Rho, Arf/Arl, Ran and Rab. G-proteins of the Arf (ADP-ribosylation factor) family are major regulators of membrane traffic and organelle structure in eukaryotic cells (14,15). In mammals, there are six Arf proteins divided into three classes based on sequence homology. They have a conserved myristoylated amino-terminal amphipathic helix which ensures membrane association and they share three functionally important regions called Switch1, Switch2 and

Inter-switch. These Switches undergo conformational changes upon nucleotide exchange and are implicated in interactions. Arf1 is found in all eukaryotes examined to date (16) and a physiological role in cell migration and in breast cancer progression has been recently reported (17). The GDP/GTP nucleotide exchange of Arf1 is under control of GEFs, such as Arno proteins (Arno, Cytohesin and Grp1). These Arno proteins share a conserved catalytic Sec7 domain of about 200 residues followed by a pleckstrin homology (PH) domain responsible for membrane targeting (18-20). Sec7 domains form an elongated superhelix of helices with an N-terminal subdomain, carrying the catalytic glutamic residue E156, and a C-terminal subdomain that closes up when associated with Arf1. Well resolved structures of Arf1 bound to GDP and GTP (21-23), isolated Sec7 domains (24) and free-nucleotide Arf1-Sec7 domain complex are available (25). Moreover, uniquely to G proteins, transient GDP-bound Arf1-GEF intermediates have been reported, using a charge reversal Arno mutant (Glu₁₅₆ to Lys) preventing the GDP release (26) or by using the natural inhibitor Brefeldin A (BFA) (26). These structural studies illustrate the conformational rearrangements and mechanisms that conduct to the formation of a binary Arf1-Sec7 complex. BFA is a fungal toxin that acts on BFA-sensitive Sec7 domain through an unusual uncompetitive mechanism and was described as an interfacial inhibitor (27). BFA binds to the protein - protein interface of the transient Arf1-GDP-Mg²⁺-Sensitive Sec7 complex and freezes it in an abortive conformation in which the GDP is maintained out of reach from the GEF catalytic site and its critical residue Glu₁₅₆ within a hydrophilic loop. Without BFA, the Glu₁₅₆ destabilizes the GDP molecule bound to Arf1 through the displacement of the Mg²⁺ ion and by repulsing the GDP β-phosphate (28). Several studies suggest that the free-Mg²⁺ G protein-GDP intermediate is the precursor prior to GDP ejection which results in a binary G protein-GEF complex with enhanced affinity (11,29).

However, Mg²⁺ departure is not a prerequisite event for the binding of Arno to Arf1 as shown in the presence of BFA, where an abortive complex is made up with the two proteins, the GDP and the cation as indicated in Scheme 1.

Thus, the interaction between Arf1 and Sec7 domains, and the stabilization of a binary Arf1-Sec7 domain complex, is allosterically regulated by natural factors or reoriented to an abortive pentameric complex in presence of BFA. However, allosteric modifications of kinetic binding parameters were still unknown.

Here, we used a Surface Plasmon Resonance (SPR) approach for measuring the kinetic parameters that govern Arf1-Arno interaction using mono-biotinylated version of [Δ 17]Arf1 and Arno Sec7 domains. We then investigated the dynamics of association/dissociation of Arf1-Sec7 domain complex and their modulations by natural allosteric factors as well as by the uncompetitive toxin BFA. This strategy allowing the identification in real time of nature and fate of complexes provides a very informative analysis at qualitative and quantitative levels that should help to solve the inhibitory mechanism of new family of inhibitors of GEF Sec7 domains.

Materials and Methods.

BODIPY® TR GTP, Guanosine 5'-triphosphate, BODIPY® TR 2'-(or-3')-O-(N-(2-aminoethyl)urethane) was purchased from Invitrogen (France). BFA, GDP sodium salt and GTP lithium salt were purchased from Sigma (St. Louis, MO).

Bacterial Strains and Plasmids

Escherichia coli DH5 α strain was used as a host for plasmid construct encoding BirA and *E. coli* BL21 (DE3) strain (Novagen, Madison, WI, USA) was used as a host for protein expressions and *in vivo* biotinylation of proteins bearing the AviTag peptide (MSGLNDI FEAQKIEWHE) (30,31). The plasmid pCDFDuet was used for the expression of BirA. The plasmid pET42 was used for the expression of N-terminal truncated human Arf1 (residues 17-181, [Δ 17]Arf1) with or without an N-terminal AviTag. The plasmid pET28-a which confers to proteins an N-terminal polyhistidine tag was used for the expression of Sec7 domains

bearing the AviTag peptide. All the plasmids were from Novagen, (Madison, WI, USA).

Cloning, Protein Expression and Purification.

All the proteins except BirA were obtained from expression of synthetic genes with optimized codons for expression in *E. coli* (Geneart, Germany). The synthetic genes coding for the Sec7 domain of human Arno (residues 50-250, Arno) or a mutant carrying four BFA-sensitizing mutations (F190Y/A191S/S198D/P208M, Arno4M) (32) were used to produce nucleotide-exchange factors used in kinetic measurement experiments. Variants of those synthetic genes encoding the additional Avitag sequence (33) in the N-Terminal region were also purchased (Geneart) to produce biotinylated-AviTag-Arno and AviTag-Arno4M proteins used in SPR experiments. The biotinylated version of G protein or GEF Sec7 domains were engineered using an AviTag construct based on the introduction of a N-terminal peptide sequence that can be enzymatically mono-biotinylated at its internal lysine residue by *E. coli* biotin protein ligase (BirA). The AviTag sequence does not resemble the consensus sequence of natural occurring biotinylation sites but is derived from an *in vitro* screen of peptide libraries (30,34).

All synthetic genes are flanked by 5' NdeI and 3' BamHI restriction sites. They were originally cloned into pMA-T and then into pET28-a vectors. The resultant plasmids pET28-a confer to proteins a polyhistidine tag and a cleavage site for Thrombin before the Avitag sequence. The cDNA encoding for [Δ 17]Arf1, digested with NdeI and BamHI, was introduced into the plasmid pET42 using T4 DNA ligase. The pCDFDuet vector (Novagen) was engineered to allow the expression of efficiently *in vivo* biotinylated recombinant proteins in *E. coli*. Briefly, the BirA gene (accession number AF044308.1) from the *E. coli* genomic DNA (strain JM109, Promega) was amplified by PCR using primer BirAFor 5'-ATGAAGGATAACACCGTGCCACTG and BirARev 5'-

TTATTTTCTGCACTACGCAGGGATATTTTC and Phusion proofreading DNA polymerase (Finnzymes). After 15 min incubation at 72°C in the presence of ThermoPol Taq polymerase (New England Biolabs) to append 3' Adenosine, the PCR fragment was cloned in pCR II (Invitrogen) and then transformed in TOP10F'. Then by PCR, the gene BirA was amplified with oligonucleotides 5'-CA[^]TATG- BirA -3' forward and 5'- BirA - GAA-AAA -TAA-C[^]TCGAG- 3' reverse containing the NdeI restriction site and the "E-K- stop codon-

XhoI restriction site respectively. The amplified BirA gene was introduced into the pcfDUET expression vector (Novagen) by digestion with both NdeI and XhoI and the ligation was performed using T4 DNA ligase. The sequencing of the gene BirA has indicated that nucleotides coding for two C-terminal amino-acids (E and K) as well as for a stop codon were missing.

[Δ 17]Arf1 protein, in its GDP form, as well as Arno and Arno4M proteins were expressed and purified as previously described (32,35) except that for Sec7 domains used in nucleotide exchange tests, the polyhistidine tag was cleaved using thrombin. Biotinylated [Δ 17]Arf1 protein was expressed using a competent strain of *E. coli* BL21(DE3) transformed with a BirA pCDFDuet expression vector and purified as previously described (35). All polyhistidine tag biotinylated Sec7 constructs were expressed and purified as followed. Briefly, *E. coli* BL21(DE3) strain transformed with pET28-a plasmids were grown at 37 °C in Luria-Bertani (LB) broth supplemented with 50µg/ml Kanamycin and 50µg/ml of streptomycin until OD_{600nm} reached approximately 0.5. Protein expression was induced with 0.4 mM isopropyl b-D-thiogalactoside (IPTG) at 18 °C for 20 h in the presence of biotine (40µM) in the media. Cells were harvested by centrifugation and resuspended in 4 ml of phosphate-buffered saline supplemented with 1% Triton X-100 and a cocktail of protease inhibitors (Roche). Cells were lysed by sonication and debris was removed by centrifugation at 35,000 rpm for 30 min. The resulting Sec7 protein solutions were filtered through a 0.22-µm filter and loaded onto a 5-ml HiTrap chelating HP column (GE Healthcare, Piscataway, NJ, USA) equilibrated with lysis buffer (Tris 50 mM, NaCl 100 mM, 2mM βME, MgCl₂ 1mM, pH 8). The resin was washed with 10 column volumes of lysis buffer after loading and eluted with a linear gradient of imidazole from 20 to 300 mM in the same buffer. Peak fractions were analyzed by 10% sodium dodecyl sulfate-polyacrylamide gel electrophoresis (SDS-PAGE). Positive fractions were pooled, desalted on a HiPrep™ 26/10 Desalting column, and concentrated with spin concentrators (Amicon Ultra- 15, molecular weight cutoff 10,000 Da, Millipore, Billerica, MA, USA). The biotin incorporation of the purified proteins was additionally confirmed by Western blot with the Streptavidin-HRP conjugate for detection of biotinylated proteins and Maldi mass spectrometry

which have shown >95% of mono-biotinylated proteins.

Kinetics Measurements of Nucleotide Exchange.

All kinetics experiments were performed with a soluble Arf1 protein truncated of the N-terminal helix, which is not dependent on lipids for nucleotide exchange, and loaded with GDP before the experiments as previously described (35), on a multimode reader *Mithras* LB 940 (Berthold). Activation of $[\Delta 17]$ Arf1 was monitored for the indicated time period by fluorescence of the guanosine 5'-triphosphate, BODIPY, 2'-(or-3')-O-(N-(2-aminoethyl)urethane) (excitation, 580 nm; emission, 620 nm) (Bodipy-GTP). All measurements were performed at 30°C in 50 mM Tris (pH 8), 50 mM NaCl, 1 mM MgCl₂, 2 mM 2-mercaptoethanol in the presence of 1 μM of $[\Delta 17]$ Arf1-Mg²⁺-GDP, and 1 μM of Bodipy-GTP, with nucleotide exchange factors and BFA at indicated concentrations. The inhibitor Brefeldin A (BFA) was incubated for 5 min before initiating the reaction with Bodipy-GTP. The spontaneous exchange of $[\Delta 17]$ Arf1 was followed in the presence of 1 μM of Bodipy-GTP and no GEF. To confirm the uncompetitive mechanism of BFA on His-AviTags-Arno4M, enzyme activity of ARNO4M was determined at substrate concentrations $[\Delta 17]$ Arf1 ranging from 0.5 to 5 μM with several concentrations of BFA (0, 5, 10, 50 and 100 μM). Fluorescence data were fitted by using the program Origin 7.03 (Microcal, Northampton, MA). All values are means ± one standard deviation of at least three independent experiments. Initial velocity of the nucleotide exchange reaction in function of BFA concentration was determined and the results were represented using the Michaelis–Menten plot and analyzed by the Lineweaver-Burk of saturation curves. Data were fitted with Michaelis-Menten equation using GraphPad software.

To study the effect of His-AviTags on Arno/4M to equilibrium binding constant Arf1 binding, anisotropy binding profiles were obtained from the titration of Alexa488-labeled $[\Delta 17]$ Arf1-GDP with Arno/4M bearing or not the His-AviTags (35).

Surface Plasmon Resonance Analysis of complexes formation. Experiments were performed on a Biacore 3000 apparatus (GE Healthcare, Uppsala, Sweden) at 25 °C in 50 mM Tris (pH 8.0), 150 mM NaCl, various concentrations of MgCl₂ and free Mg²⁺ as indicated, 2 mM BME, 0.005% P20 as running buffer at a flow rate of 50 μl/min. Using biotin capture kit (GE Healthcare), biotinylated

$[\Delta 17]$ Arf1 and HisTag-biotinylated-Arno or Arno4M were captured on CAP sensor chip according to the manufacturer's instructions. The immobilization levels are given in the figures and tables captions. A control surface was prepared with the same protocol without the protein. After the capture of the biotinylated protein the surfaces were saturated with an injection of biotin (40 μg/ml). For the kinetic analysis of Arf1 on immobilized Arno: increasing concentrations of Arf1 solutions (12.5 nM to 1600 nM) were injected on immobilized Arno or Arno 4M during 180s followed by a dissociation of 400s. Arno coated surfaces were regenerated with a pulse (30s) of GDP (2 μM) which rapidly destabilizes the complex. For the reverse kinetics biotinylated Arf1 were captured on Cap sensor chip (200-380 RU) increasing concentrations (25 nM to 1600 nM) of Arno or Arno 4M were injected. Between each run, the surface was fully regenerated with a mixture (3/1:v/v) of 8M guanidine hydrochloride and 1M sodium hydroxide (GE Healthcare). The necessity of repetitive immobilizations of Arf1, which differ from a simple regeneration of immobilized Sec7 domain by GDP (Figure 4), results from a conformation instability of Arf1 when immobilized which could be due to a time dependent protein unfolding associated with the nucleotide departure (data not shown). The regenerability of the surface by repetitive immobilization of Arf1 avoids the problem to occur. To investigate the influence of AviTag on $[\Delta 17]$ Arf1 to the binding with Arno, the Sec7 domain was covalently bound at high level to the carboxymethyl dextran CM5 sensor chip surface, then $[\Delta 17]$ Arf1 with or without the AviTag was injected at 50 nM during 180s followed by a dissociation time of 400s. (data not shown). To obtain a 1 μM concentration of Mg²⁺, 1 mM of MgCl₂ were mixed to 2 mM of EDTA and combined extemporaneously with Arf1 during sample injection (36).

All sensorgrams were corrected by subtracting the response from the control reference surface. The kinetic parameters were globally fitted with a 1:1 Langmuir binding (A+B = AB) or heterogeneous ligand-parallel reaction model (parallel reactions, A+B1 = AB1, A + B2 = AB2) by using BIAevaluation version 4.2 software (Biacore software handbook C16-C18). The absence of mass transfer limitation was checked for kinetics analysis. Kinetic constants are the result of at least three independent set of experiments. The validity of the fit was given by the χ^2 factor less than 10% of the Rmax value. According to the manufacturer's

instructions the T value was greater than 10 for all the given fitted parameters (T value is obtained by dividing the value of the parameter by the standard error). The stoichiometric ratio (SR) is the ratio between the observed maximum binding response (Rmax) and the calculated maximum binding response (calcRmax). calcRmax is given by the molecular mass ratio of analyte to ligand, multiplied by the stoichiometry of 1 and the amount of immobilized ligand.

$$SR = \frac{R_{max,exp}}{R_{max,calc}} \quad \text{Equation 1}$$

$$R_{max,calc} = R_{u,immobilized-level} \times \frac{MW_{analyte}}{MW_{ligand}}$$

Results.

According to previous reports on nucleotide allosteric competition (9,37), scheme 1 shows a simplified model of the catalyzed GDP release from Arf1 upon the formation of a transient quaternary complex which leads to a binary Arf1-Arno complex with enhanced binding affinity. Additional steps with the release of Mg^{2+} as well as the conformational changes of Arf1 are not indicated. With BFA and for sensitive Sec7 domains, a pentameric complex has been crystallized which corresponds to an abortive form where the catalyzed release of GDP by Sec7 domain is impaired (11,26,38,39). Scheme 1 indicates the rate constants delineating each association (k_{a1} to k_{a6}) or dissociation (k_{d1} to k_{d6}) steps. The SPR approach allows us to measure some of these rate-constants giving a comprehensible flow chart that will be described in the following sections. In our study, we used a soluble truncated version of Arf1, lacking the 17 N-terminal amino-acid residues that are crucial for membrane insertion, which is fully active in catalyzed nucleotide exchange without the requirement of protein-phospholipid interactions and targeted by BFA in a Sec7 dependent manner (25,35,39). Sec7 domain of Arno is considered as a representative of BFA-resistant Arf-GEFs and sensitivity to BFA was engineered by mutation of Phe¹⁹⁰, Ala¹⁹¹, Ser¹⁹⁸ and Pro²⁰⁸ to Tyr, Ser, Asp and Met, respectively (38).

I) The biotinylation of the proteins does not change the nucleotide exchange catalysis and the apparent equilibrium dissociation constant of Sec7 domains to [Δ 17]Arf1.

To perform SPR studies, proteins were immobilized on a new sensor chip that allows the reversible capture of biotinylated proteins and regeneration of the ligand (40). In order to circumvent deleterious effect of N-terminal additional Tags, we compared the nucleotide exchange of [Δ 17]Arf1 (Scheme 2) and its mono-biotinylated-AviTag version under stimulation by BFA-resistant and BFA-sensitive Sec7 domains (later referred to as Arno and Arno4M, respectively) bearing or not mono-biotinylated-His-AviTags at the N-terminus (Figure 1). The apparent inhibition constants (K_{iapp}) of BFA for Arno and Arno4M with or without additional mono-biotinylated Tags were determined. For His-AviTags-Arno4M, Arno4M, His-AviTags-Arno and Arno, K_{iapp} are respectively $16 \pm 5 \mu M$, $11 \pm 4 \mu M$, $454 \pm 226 \mu M$ and $291 \pm 45 \mu M$ (Figure 1, Panel B) which indicate an equivalent sensitivity to BFA regardless of the presence of mono-biotinylated Tags and were in good agreement with previous reports (32,41). The inhibition on AviTags-Arno4M activity in function of BFA concentration using a Michaelis–Menten plot is reported on Figure 1, Panel C. The derived Lineweaver-Burk plot gave parallel lines (data not shown) which confirmed the uncompetitive inhibition mechanism of BFA on the His-AviTags-Arno4M exchange activity (35,42). At last, the non-interference of additional mono-biotinylated-AviTag on [Δ 17]Arf1 was confirmed by comparison with spontaneous and catalyzed nucleotide exchanges of free-Tag [Δ 17]Arf1 version (Figure 1, Panel D).

From this, we concluded that additional His-Tag or mono-biotinylated-AviTag do not affect, neither the ability of GEFs to accelerate the nucleotide exchange on Arf1 nor the sensitivity to the uncompetitive inhibitor BFA. We then compared the equilibrium dissociation constant of [Δ 17]Arf1 to Arno/4M and mono-biotinylated-His-AviTags-Arno/4M by fluorescence

anisotropy as previously described (35) and found apparent K_{DS} were similar in the 20 nM range (data not shown). Therefore, these tagged-proteins behave similarly to their untagged versions and were used in the SPR experiments.

II) Interaction of [$\Delta 17$]Arf1-GDP on immobilized Arno and Arno4M conducts to a binary complex.

Our first aim was to investigate the interaction of [$\Delta 17$]Arf1-Mg²⁺-GDP to BFA-resistant and BFA-sensitive biotinylated Sec7 domains using SPR technique at 25°C, pH 8 and 150 mM NaCl. The formation of the binary Arf1-Arno complex was also studied through the action of the effectors Mg²⁺ ion and nucleotides. As indicated in the schematic representation (Figure 2), using a CAP Sensor Chip, biotinylated-AviTag constructs of Sec7 domains were immobilized on streptavidin conjugated with a ss-DNA oligo. An immobilization level of 200-600 resonance units (RU) was found as a good compromise to get enough RU binding levels with Arf1-Mg²⁺-GDP and kinetic constants devoid of rebinding and non-specific effects (data not shown). As previously described (35), [$\Delta 17$]Arf1 is obtained in its GDP conformation when purified in the presence of GDP and MgCl₂. Moreover, for the present study, the GDP-bound conformational state of the purified protein has been monitored through N-¹H HSQC NMR spectra using ¹⁵N labeled [$\Delta 17$]Arf1 (data not shown). To strengthen the nucleotide binding to Arf1 and to maintain a stable [$\Delta 17$]Arf1-Mg²⁺-GDP association, capture, sample and running buffers were supplemented with 1mM MgCl₂ (10,43). SPR kinetic sensorgrams of [$\Delta 17$]Arf1-Mg²⁺-GDP association with and dissociation from are shown in Figure 3, panel A where the G protein was injected at increasing concentrations from 50 nM to 1600 nM. Between injections of Arf1-Mg²⁺-GDP, regeneration of Sec7 domains was realized by a pulse of 2 μ M GDP. Using Biaevaluation software and a Langmuir 1:1 binding model, the association-rate constant (k_a) for the

complex was determined to be 219000 M⁻¹ s⁻¹, the dissociation-rate constant (k_d) to be 0.0041 s⁻¹ and the k_d/k_a ratio was 19 nM with a χ^2 of 1.3 (Table 1A). In accordance with the allosteric competition between nucleotides and GEFs for the binding to G proteins as well as previous reports (9,44), the complex observed in this first experience is assumed to correspond to the free nucleotide Arf1-Arno complex (named binary complex in scheme 1) (44,45). As the terms affinity and equilibrium constant (K_D) of a complex referred to association/dissociation of two equivalent partners and because, in this SPR experiment, the association occurs with Arf1-GDP whereas the dissociation is related to Arf1, in its free nucleotide form, we reported for each complex observed, the k_d/k_a ratio to illustrate the complex stability.

With immobilized Arno4M, similar association/dissociation profiles were obtained with a k_d/k_a ratio of 18 nM and a χ^2 of 1.09 (Figure 3, Panel B, Table 1A). Kinetic parameters of interactions with the two Sec7 domains are equivalent which indicate the 4 mutations on Arno4M have no influence on the association with the G protein. Considering a ratio of 1:1 for the binding of Arf1 to a Sec7 domain, the stoichiometric ratio (SR) represents the percentage of detected complexes over the theoretical number of possible complexes. SR was estimated from the ratio of the experimental R_{max} on the calculated R_{max} (Equation 1 in Materials and Methods) and revealed a SR with values of 0.3 and 0.27 for Arno and Arno4M respectively (Table 1A). We also examined the sensitivity of kinetics parameters to temperature, salt and pH have been evaluated using immobilized Arno within another set of experiments. As shown, on Table 1B, a decrease of the experimental temperature from 25 to 10 °C conducts to a progressive loss of the SR value. Whereas SPR experiments performed at pH7 or in the presence of 300 mM of NaCl revealed that initial conditions conferred the highest association rate (k_a on Table 1C).

III) Effect of Mg^{2+} on the interaction between [$\Delta I7$]Arf1 and Arno.

We performed a set of experiments to investigate the influence of free Mg^{2+} on kinetic parameters of the interaction between [$\Delta I7$]Arf1 and Sec7 domain as the removal of the cation accelerates by a factor of 20 the spontaneous nucleotide departure giving the binary G protein-GEF complex (10,36). [$\Delta I7$]Arf1- Mg^{2+} -GDP, with or without a 10 min preincubation of 10mM EDTA, was run over on immobilized Arno (500 RU). The sensorgrams obtained from three independent trials are given in Figure 3, panel C & D and in both case, the kinetics are fitted with a Langmuir1:1 reversible binding model. In standard conditions with 1mM $MgCl_2$ (Figure 3, Panel D), the kinetic constants (k_a : 166000 $M^{-1} s^{-1}$, k_d 0.0038 s^{-1}) were similar to data of Figure 3, panel A (Table 1A& 2) which underlines the highly reproducible level of measured constants. When free Mg^{2+} was removed by EDTA, an increase of the k_a by a factor of 2.37 was observed and no effect was noted on the dissociation-rate constant which confirm the influence of this cation on [$\Delta I7$]Arf1 and Sec7 domain association. Moreover, the absence of free Mg^{2+} induced an increase of the SR value at 68% (to be compared to 32% with 1mM $MgCl_2$, Table 1A& 2).

It turns out that the absence of Mg^{2+} destabilizes the nucleotide binding and enhances the spontaneous nucleotide release, and so we cannot rule out that changes in k_a and SR values came from a nucleotide-free Arf1 population generated during the 10 min. incubation with EDTA. However, the statistical analysis with a χ^2 value around 10% of the Rmax rather suggests that Arf1 is still homogenous in term of population which is more compatible with a bound-GDP G protein state. To confirm the influence of Mg^{2+} on kinetic constants, we performed several kinetic titration experiments by injecting [$\Delta I7$]Arf1-GDP, from 25 to 400 nM, at 1mM and 1 μ M of Mg^{2+} on immobilized Arno (500 RU) (Table 3). With a langmuir1:1 reversible binding model, we found the effect of the lowest

Mg^{2+} concentration to be similar to that of the EDTA preincubation experiments, with a 2.2-fold enhancement of the association-rate constant, no appreciable change of the dissociation-rate constant and a sharp increase of the percentage of complex formation.

IV) Reverse system to study the association of Arno to [$\Delta I7$]Arf1.

The next step was an attempt to determine the kinetic parameters of Arf1-Arno complex association/dissociation starting from a free-nucleotide Arf1 population, corresponding to the step defined by k_{a4} and k_{d4} (Scheme 1). Thus, we set a reverse SPR strategy on immobilized biotinylated [$\Delta I7$]Arf1. As indicated in Figure 4, the biotinylated-AviTag construct of [$\Delta I7$]Arf1 was repetitively immobilized on streptavidinconjugated with a ss-DNA oligo up to a level of ~370 RU.

Then, to generate a free-nucleotide Arf1 population, immobilized G- protein was washed 10min with a 10mM EDTA running buffer according to a previous report (44). Arno was injected at concentrations from 6.25 nM to 1600 nM with Arf1-coated to the surface fully regenerated between two Arno injections. In the presence of 1mM $MgCl_2$, curve analysis was compatible with a stoichiometric Langmuir 1:1 binding model with a k_a of 26600 $M^{-1} s^{-1}$, k_d of 0.0055 s^{-1} and the k_d/k_a ratio was around 200 nM with a χ^2 of 6.37. The SR value was 0.91 (Table 4). It is worthy to note that the k_a obtained with immobilized Arf1 is about 10-fold lower compared with immobilized Arno (Tables 1 & 2); however the percentage of complex formation is 3-fold higher (0.91 versus 0.32).

After treatment of immobilized [$\Delta I7$]Arf1 with EDTA, data analysis showed that a stoichiometric Langmuir 1:1 binding model was no more adequate but instead revealed the adequation with a heterogeneous ligand binding model with 2 interacting populations, each representing around 50% (Table 4). A high stable population with a k_d/k_a ratio of 44 nM and another population with a k_d/k_a ratio of 338 nM. The percentage of

population with high stability was not increased by an extending EDTA washing time; even this would tend to destabilize the bioactive conformation of the G protein (data not shown).

As the association-rate constant of the binary Arf1-Arno complex with G protein immobilized is lower than that obtained with immobilized Arno and also due to a drastic difference of the SR value, it was not possible to precise the influence of GDP on kinetic binding parameters, particularly k_{a4} and k_{d4} , of complex formation. In order, to understand these changes, mono-biotinylated-AviTag- $[\Delta 17]$ Arf1 and $[\Delta 17]$ Arf1 were assayed on immobilized Arno covalently bound to the surface of CM5 chip (the CM5 allows to use flowing biotinylated proteins). In this case with Biot-AviTag- $[\Delta 17]$ Arf1, the k_a and SR are decreased by a factor of ~ 2 when compared to $[\Delta 17]$ Arf1 (data not shown) which indicates that the additional Tag has a negative impact for the binding to Arno and could explain the lower association-rate constant obtained with immobilized Arf1 compared to immobilized Arno. It has to be noted that no influence of additional Tags on Arno/4M to the binding with Arf1 were detected as described above.

The instability of Arf1 and the negative impact of Avitag on kinetics parameters for immobilized Arf1 clearly indicate that the approach using immobilized Arno has to be privileged.

V) GDP and GTP counteract the Arf1-Arno complex detection with the same potency.

The nucleotide exchange activity of a GEF is not specific to the Arf1-GDP form and Arf1-GTP to GDP exchange is also stimulated by GEFs (26,44). According to the allosteric model presented in the introduction, both nucleotides counteract the stability of the binary G protein-GEF complex (9). With Arf1 and GEF Sec7 domains, this deleterious effect is illustrated on Figure 5, Panel A, which shows in the presence of 2 μ M GDP the drastic disappearance of binary complex detection with immobilized Arno or Arno4M

and Arf1 at 200 nM. The same effect was observed with GTP (sensorgram not shown). To investigate the relative potency of GDP and GTP to interfere on the Arf1-Arno complex stability, we measured at equilibrium the RU plateau levels of complex formation on immobilized Sec7 domains in the presence of various nucleotide concentrations. $[\Delta 17]$ Arf1 was in the flow at concentration of 800 nM. As shown for Arno on Figure 5, Panel B, the same decrease in binding levels was observed for both nucleotides with an half effect at 179 \pm 20 nM and 140 \pm 20 nM for GDP and GTP, respectively. A comparable result was obtained with immobilized Arno4M (data not shown).

VI) Interaction of immobilized Arno and Arno4M with Arf1-Mg²⁺-GDP in the presence of BFA and GDP.

The next goal of our study was to investigate the modifications induced by the uncompetitive inhibitor BFA on kinetic parameters of the interaction between Arf1-Mg²⁺-GDP and GEF sec7 domains. As already mentioned, with BFA-sensitive Sec7 domain, the toxin freezes in an abortive conformation the pentameric protein-protein complex with Mg²⁺, GDP and BFA part of the association (38,39,42). The simplified mechanism for the formation of the pentameric complex is represented in Scheme 1 (light blue) as previously described (38), however the way this complex dissociates is not completely elucidated. Previous experiments from Figures 3&5 revealed that Arno and Arno4M presented the same association/dissociation profile with the G protein and that the binary complex detection with 200 nM $[\Delta 17]$ Arf1 was abolished by 2 μ M GDP. However, as indicated on Figure 6, Panels A & B, despite the presence of 2 μ M GDP, BFA at 100 μ M during the association phase restores the complex detection for both Sec7 domains, with a major effect on immobilized Arno4M compared to Arno (Table 5) as judged by the SR value. With Arno4M, the analysis of kinetic data fitted well with a langmuir1:1 reversible binding model. The k_a value of 6270

$M^{-1} s^{-1}$ and the k_d value of $0.00032 s^{-1}$ (Table 5) are reduced by a factor of 42 and 15, compared to values found without GDP and BFA, and the k_d/k_a ratio was 52 nM (Table 5). In another set of experiments, GDP was also present during the protein dissociation phase and comparable kinetic constants were obtained, particularly the same dissociation-rate constant ($0.00036 s^{-1}$) indicating that the nucleotide has no or little influence on complex dissociation (data not shown). Analysis of the SR revealed that the complex formation reached 79% (Table 5). The binding level increases proportionally to the concentration of BFA (data not shown) with 100 μM the higher concentration investigated which is around 10-fold the K_{iapp} of the toxin (Figure 1). The kinetic data obtained in the presence of BFA and GDP are compatible with the formation and stabilization of a pentameric $[\Delta I7]Arf1-Mg^{2+}-GDP-BFA-Arno4M$ complex (see discussion). This effect was expected for Arno4M since the four mutations confer sensitivity to the toxin and allow the formation of an abortive pentameric complex (38,39,42).

With Arno, in the presence of BFA and GDP during the association phase, data analysis of complex detection revealed that a Langmuir 1:1 reversible binding model is not suitable and rather curves fitted with a heterogeneous binding model showing two almost equal populations of complexes in the range of 19 % (Figure 6, Panel A, Table 5). A first population is characterized by a k_{a1} value of $4620 M^{-1} s^{-1}$ and a k_{d1} value of $0.0015 s^{-1}$ corresponding to an equivalent association-rate constant and a 20-fold higher dissociation-rate constant when compared to Arno4M. These values suggest that Arno and Arno4M Sec7 domains both associate to form a pentameric $[\Delta I7]Arf1-Mg^{2+}-GDP-BFA-Sec7$ -domain complex, however with a lower complex stability for Arno (k_{d1}/k_{a1} : 344 nM) due to an higher dissociation rate (see discussion). The second population of complexes obtained with Arno is more difficult to understand, it represents 50% of the amount of complexes with a higher

association-rate constant k_{a2} ($33200 M^{-1} s^{-1}$), a very rapid dissociation-rate ($0.0362 s^{-1}$) which could be assigned to a complex with likely a destabilizing effect from the bound-nucleotide.

VII) Interaction of immobilized Arno and Arno4M with Arf1- Mg^{2+} -GDP in the presence of BFA but no GDP.

In the last part of our study, we investigated the effect of BFA on protein complex formation in the absence of the allosteric competitive action of GDP. In the presence of 100 μM BFA but no GDP in the sample solution, data analysis of the $[\Delta I7]Arf1-Mg^{2+}-GDP$ binding to immobilized Arno4M were fitted with a heterogeneous ligand binding model which encompass two types of complexes. One population with kinetic constants (k_a and k_d in the 10^5 and 10^{-3} range, respectively) which is consistent with the binary complex detection, and another set of constants compatible with the pentameric complex (k_a and k_d in the 10^3 and 10^{-5} range, respectively) (Figure 7, Panel B, Table 6). The deconvolution of individual fitting curves obtained at different Arf1 concentrations (Figure 7, Panels C, D, and E) reveals that the ratio of pentameric (AB_2) versus binary (AB_1) complex increases with the concentration of Arf1. Thus, at 25 nM of Arf1, most of the protein-protein association detected provides from the binary complex whereas at saturating concentration, the pentameric complex is the most abundant.

By contrast, without GDP in the running buffer, data analysis of binding to immobilized Arno fitted a Langmuir 1:1 reversible binding model with a complex formation of 21% (Figure 7, panel A, Table 6). In this case, values for k_a and k_d are in the 10^5 and 10^{-3} range, respectively and therefore are characteristics of the binary complex association/dissociation. It has to be noted in the absence of GDP in the association running buffer, that no pentameric complex formation was detected with BFA-resistant Sec7 domain.

Discussion.

The structure of myristoylated or non myristoylated Arf1 and $[\Delta I7]$ Arf1 bound to GDP or GTP and in complex with Sec7 domains revealed the sequential conformational changes and the role of GEFs during nucleotide exchange (21,22,24,28,36,42,46). The protein-protein interface encompasses the Switch 1 and 2 regions (residues 38-51 and 69-84, respectively) of Arf1 with the hydrophobic groove and carboxy-terminal helices of the Sec7 domain (Figure 8, up). Except for N-terminal helix, Switch and Interswitch (residues 52-68) regions, the conformation of the core of the G protein is globally the same throughout the nucleotide exchange. The myristoylated N-terminal helix is directed towards the protein core in the bound-GDP state, and is extruded mediating membrane interaction in the bound-GTP (Figure 8, pdb codes 2K5U, 1U81 versus 1O3Y). If Switch 1 shows a drastic alteration with some residues inserted into the hydrophobic surface groove of the Sec7 domain, the Switch 2 is performed on Arf1-GDP to the initial encounter with the GEF. From Arf1-GDP to Arf1-Sec7 domain complex and further in the Arf1-GTP state, strands $\beta 2$ and $\beta 3$ of the interswitch are translated up to 7 Å in the direction of the initial N-terminal helix pocket. With the toggle of the interswitch, a 20° rotation of the Arf core brings the β -phosphate of the GDP close to the catalytic E156 which enhances the nucleotide departure and conducts to a stable binary Arf1-Arno complex with a high affinity. In the presence of nucleotides, the rapid dissociation of the complex occurs upon binding of GTP, as well as GDP, which induces the release of the GEF through an allosteric mechanism, that can be considered as a simplified Ping Pong Bi Bi mechanism (47,48).

In this study, taking advantages of the regenerability of the CAP sensor chip (40) coupled with a system that allows *In Vivo* mono-biotinylation of proteins by co-expression of BirA, we developed a SPR approach to determine kinetic parameters of

the $[\Delta I7]$ Arf1 interaction to Arno Sec7 domains as well as changes induced on the type and fate of formed complexes in the presence of natural and exogenous allosteric factors.

During the association phase (Figure 8, Panel A), we observed the formation of a stable $[\Delta I7]$ Arf1-Sec7 domain binary complex with both immobilized Arno and Arno4M. The association-rate constant, close to $2 \cdot 10^5 \text{ M}^{-1} \text{ s}^{-1}$ within independent trials, corresponds to the transient Arf1-Mg²⁺-GDP-Arno complex formation (k_{a2}) followed by the departure of Mg²⁺ and GDP (k_{d3}) whereas the measured dissociation-rate constant, in the $5 \cdot 10^{-3} \text{ s}^{-1}$ range, corresponds to the dissociation of the binary complex (k_{d4}) (Scheme 1 and Figure 8, Panel A). The k_a/k_d ratio reflecting the overall complex stability was around 20 nM which could be compared to the affinity reported for some other G proteins and GEFs (eg 4.6 nM for Ras and Cdc25^{Mm285}, (9,44)). In a reverse system using immobilized free-nucleotide Arf1, we attempted to measure the k_{a4} constant of Sec7 domain binding to free-nucleotide Arf1. Unfortunately, in contrast with the study of Lenzen et al. based on immobilized Ras and flowing Cdc25^{Mm285}, it appears that the immobilization of Arf1 could interfere with the formation of a high affinity complex and causes a 10 fold decrease of the association-rate constant ($2.66 \cdot 10^4 \text{ M}^{-1} \text{ s}^{-1}$, Table 4).

The absence of free Mg²⁺ decreases the GDP and GTP binding affinity by destabilizing the coordination of the nucleotide binding site and promotes the formation of the binary G protein-GEF complex (10,12). In terms of kinetic parameters of binding, our data revealed that Mg²⁺ ion potentiates by a factor of 2 the counteracting allosteric effect of GDP on the binding of Arf1 to immobilized Sec7 domains as the absence of ions causes a ~2-fold reduction of the association-rate constant (Tables 2 & 3). Interestingly, the absence of free Mg²⁺ enhanced by a factor of ~2 the percentage of detected complexes which suggests a possible effect of Mg²⁺ on the conformation of Arf1 suitable to interact with

Arno as recently reported in a study using molecular dynamics simulations (11).

As illustrated with the nucleotide exchange assay using fluorescent labeled guanosine triphosphate (Figure 1) saturating concentrations of nucleotides did not abolish the initial binary complex formation but its stability as we observed the release of Arf1-Mg²⁺-GTP with enhanced fluorescence. With immobilized Arno and flowing Arf1, in the presence of GDP/GTP at saturating concentrations, this allosteric nucleotide effect analyzed by SPR showed that neither the transient complex nor the binary one were detected which indicated that the binary complex dissociation is very fast (Figure 5 and 8, panel BI). Moreover, there is no pronounced specificity toward the nature of the nucleotide to destabilize the binary complex as with 800 nM of flowing Arf1, 50 % of complex formation was detected at concentrations of nucleotides of 140 nM and 179 nM for GDP and GTP, respectively, in good accordance with previous reports (49).

After the characterization of kinetic parameters of the binary complex formation and the allosteric regulations by Mg²⁺ and GDP/GTP, we studied the formation of complexes induced by BFA toxin. With BFA-sensitive Sec7 domain as Arno4M, a complex, different from the binary one, is observed with a lower association-rate constant and a slower dissociation-rate constant, in the $6 \cdot 10^3 \text{ M}^{-1} \text{ s}^{-1}$ and $3 \cdot 10^{-4} \text{ s}^{-1}$ range, respectively (Table 5). As this complex was observed in the presence of GDP and in accord with the uncompetitive inhibitory mechanism of BFA, we assumed it corresponds to an abortive pentameric [Δ17]Arf1-Mg²⁺-GDP-BFA-Sec7 domain complex trapped by the inhibitor (Figure 8, Panel BII). The association-rate constant corresponds to the transient Arf1-Mg²⁺-GDP-Arno4M complex formation (k_{a2}) followed by the association of BFA (k_{a5}) (Scheme 1). It is worthy to note that whereas the k_a is reduced, the percentage of pentameric complex increased up to 79 % compared to 30% for the binary complex in standard conditions, highlighting the critical role of the

slow dissociation-rate on the pentameric complex detection (Figure 8, Panel BII). For Sec7 domains sensitive to BFA, the inhibitor freezes the complex before the release of the nucleotide and the formation of the binary complex (26,39,42). As shown on Figure 8 (pdb code 1R8Q), the BFA interacts without leading to the interswitch toggle and no rotation of the Arf1 core occurs. The role of BFA during the slow dissociation of this pentameric complex remains unknown but the dissociation of BFA has been reported as the rate-limiting step for the liberation of GDP from Arf1 (38).

In the presence of GDP and BFA, with the BFA-resistant Sec7 domain, 2 populations of complexes were observed which behave differently from the true abortive pentameric complex. First, a 19 % population displays an association-rate constant ($4.6 \cdot 10^3 \text{ M}^{-1} \text{ s}^{-1}$) equivalent to that observed with the Arno4M pentameric complex (Table 5) but a dissociation-rate constant k_{d1} ($1.59 \cdot 10^{-3} \text{ s}^{-1}$) close to the k_d found for the binary complex dissociation (eg. $4.1 \cdot 10^{-3} \text{ s}^{-1}$, Table 1). This is in complete agreement with the inhibitory mechanism of BFA as the toxin only freezes complexes which encompass a BFA-sensitive Sec7 domain. Without GDP during the dissociation-phase, BFA does not interfere with the interswitch toggle of Arf1 within the pentameric [Δ17]Arf1-Mg²⁺-GDP-BFA-Arno complex. Therefore, after the conformational change of Arf1 which ends when the GDP is released, we observe the dissociation of the binary Arf1-Arno complex in the 10^{-3} s^{-1} range (Figure 8, Panel BII). The association of BFA with complexes formed by BFA-resistant Sec7 domains has already been reported (38,39) but not the kinetic parameters and fates in real time. The second 19 % population obtained with Arno is not understood. It represents 50 % of the complex formed and has an association-rate constant k_{a2} ($3.32 \cdot 10^4 \text{ M}^{-1} \text{ s}^{-1}$) intermediate between the binary complex and the pentameric one. It has also a very fast dissociation-rate (3.61

10^{-2} s^{-1}). Due to the fast dissociation rate, one can at least suggest that allosteric effect of

GDP has a critical role in the dissociation. However, the exact nature of this complex remains puzzling.

The last set of experiments performed with BFA but in the absence of GDP during the association phase reveals the prevalence of the binary complex compared to the pentameric one. With Arno4M, we observed the formation of a heterogeneous population composed by a first complex (SR of 0.17) with a set of kinetic constants compatible with the binary complex and a more important (SR of 0.66) with parameters corresponding to the pentameric complex (Figure 8, Panel BIII). This result confirms that in the absence of nucleotide during the association phase, the binary complex is stable enough to be detected. Interestingly, in relation with respective kinetic constants, as shown in Figure 7, Panels C-D-E, the ratio between binary and pentameric complex varies upon the concentration of Arf1, the binary complex being preponderant at low concentration and the pentameric becoming prevalent at concentrations higher than 400 nM where the Rmax of the binary complex is reached.

With Arno in the absence of flowing GDP, the binary complex is detected since the allosteric competition by the nucleotide does not occur and no additional complex was observed (Figure 8, Panel BIII). The absence of the pentameric $[\Delta I7]$ Arf1-Mg²⁺-GDP-BFA-Arno complex is in accordance with the BFA-resistance characteristic of this Sec7 domain. However, the comparison with previous experiment when BFA and GDP were present in the association phase (Figure 8, Panel BII) suggests a new role of the nucleotide allosteric effect as a prerequisite for

the pentameric complex detection with Sec7 domains describe as BFA-resistant. Indeed, it seems that the uncompetitive inhibition by BFA and the nucleotide allosteric effect combine to stabilize an abortive complex as long as the nucleotide remains present. The relevance of such Arno pentameric complex in a cellular context is unknown but on purified BFA-resistant Sec7 domains an inhibition was observed with high concentrations of BFA as shown on Figure 1.

In recent years beside BFA, several inhibitors have been identified for G proteins of the Arf sub-family and their GEFs through polarization displacement fluorescence assay (SecinH3, (50)), In Silico approach (LM11, (35)), and phenotypic high-throughput screens (Golgicide A (51), Exo2, LG186, (52), AG1478, Amf-26, (53)). These compounds, with several present some specificity for a GEF (eg. GBF1), have clearly underlined the putative potential of these proteins as therapeutic targets. However, except the uncompetitive inhibitor BFA, their inhibitory mechanisms are not clearly understood, in part due to the fact that these compounds are not very active in a nucleotide exchange assay on purified proteins. Moreover, structural data with the modes of binding of these compounds are not available which impaired oriented molecular optimizations. Here, the SPR approach with identification in real time of nature and fate of complexes allows a very informative analysis at qualitative and quantitative levels that should help to solve the inhibitory mechanism of new family of inhibitors.

References

1. Rojas, A. M., Fuentes, G., Rausell, A., and Valencia, A. *The Journal of cell biology***196**(2), 189-201
2. Wennerberg, K., Rossman, K. L., and Der, C. J. (2005) *Journal of cell science***118**(Pt 5), 843-846
3. Heasman, S. J., and Ridley, A. J. *Small GTPases***1**(3), 174-179
4. Heasman, S. J., and Ridley, A. J. (2008) *Nature reviews***9**(9), 690-701
5. Vigil, D., Cherfils, J., Rossman, K. L., and Der, C. J. *Nat Rev Cancer***10**(12), 842-857
6. Rossman, K. L., Der, C. J., and Sondek, J. (2005) *Nature reviews***6**(2), 167-180
7. Klebe, C., Prinz, H., Wittinghofer, A., and Goody, R. S. (1995) *Biochemistry***34**(39), 12543-12552
8. Guo, Z., Ahmadian, M. R., and Goody, R. S. (2005) *Biochemistry***44**(47), 15423-15429
9. Goody, R. S., and Hofmann-Goody, W. (2002) *Eur Biophys J***31**(4), 268-274
10. Pan, J. Y., and Wessling-Resnick, M. (1998) *Bioessays***20**(6), 516-521
11. Hamida-Rebai, M. B., and Robert, C. H. *PloS one***5**(2), e9142
12. Zhang, B., Zhang, Y., Wang, Z., and Zheng, Y. (2000) *The Journal of biological chemistry***275**(33), 25299-25307
13. Rao, Y., Bian, C., Yuan, C., Li, Y., Chen, L., Ye, X., Huang, Z., and Huang, M. (2006) *Biochemical and biophysical research communications***348**(3), 908-915
14. Nie, Z., Hirsch, D. S., and Randazzo, P. A. (2003) *Current opinion in cell biology***15**(4), 396-404
15. Casanova, J. E. (2007) *Traffic (Copenhagen, Denmark)***8**(11), 1476-1485
16. Donaldson, J. G., and Jackson, C. L. *Nature reviews***12**(6), 362-375
17. Boulay, P. L., Schlienger, S., Lewis-Saravalli, S., Vitale, N., Ferbeyre, G., and Claing, A. *Oncogene***30**(36), 3846-3861
18. Jackson, C. L., and Casanova, J. E. (2000) *Trends in cell biology***10**(2), 60-67
19. Moss, J., and Vaughan, M. (2002) *Archives of biochemistry and biophysics***397**(2), 156-161
20. Kolanus, W. (2007) *Immunological reviews***218**, 102-113
21. Amor, J. C., Harrison, D. H., Kahn, R. A., and Ringe, D. (1994) *Nature***372**(6507), 704-708
22. Greasley, S. E., Jhoti, H., Teahan, C., Solari, R., Fensome, A., Thomas, G. M., Cockcroft, S., and Bax, B. (1995) *Nature structural biology***2**(9), 797-806
23. Ihara, K., Muraguchi, S., Kato, M., Shimizu, T., Shirakawa, M., Kuroda, S., Kaibuchi, K., and Hakoshima, T. (1998) *The Journal of biological chemistry***273**(16), 9656-9666
24. Cherfils, J., Menetrey, J., Mathieu, M., Le Bras, G., Robineau, S., Beraud-Dufour, S., Antonny, B., and Chardin, P. (1998) *Nature***392**(6671), 101-105
25. Goldberg, J. (1998) *Cell***95**(2), 237-248
26. Renault, L., Guibert, B., and Cherfils, J. (2003) *Nature***426**(6966), 525-530
27. Pommier, Y., and Cherfils, J. (2005) *Trends in pharmacological sciences***26**(3), 138-145

28. Kremer, W., Steiner, G., Beraud-Dufour, S., and Kalbitzer, H. R. (2004) *The Journal of biological chemistry***279**(17), 17004-17012
29. Soundararajan, M., Turnbull, A., Fedorov, O., Johansson, C., and Doyle, D. A. (2008) *Proteins***72**(1), 498-505
30. Smith, P. A., Tripp, B. C., DiBlasio-Smith, E. A., Lu, Z., LaVallie, E. R., and McCoy, J. M. (1998) *Nucleic acids research***26**(6), 1414-1420
31. O'Callaghan C, A., Byford, M. F., Wyer, J. R., Willcox, B. E., Jakobsen, B. K., McMichael, A. J., and Bell, J. I. (1999) *Analytical biochemistry***266**(1), 9-15
32. Zeeh, J. C., Zeghouf, M., Grauffel, C., Guibert, B., Martin, E., Dejaegere, A., and Cherfils, J. (2006) *The Journal of biological chemistry***281**(17), 11805-11814
33. Kumano-Kuramochi, M., Xie, Q., Sakakibara, Y., Niimi, S., Sekizawa, K., Komba, S., and Machida, S. (2008) *J Biochem***143**(2), 229-236
34. Beckett, D., Kovaleva, E., and Schatz, P. J. (1999) *Protein Sci***8**(4), 921-929
35. Viaud, J., Zeghouf, M., Barelli, H., Zeeh, J. C., Padilla, A., Guibert, B., Chardin, P., Royer, C. A., Cherfils, J., and Chavanieu, A. (2007) *Proceedings of the National Academy of Sciences of the United States of America***104**(25), 10370-10375
36. Beraud-Dufour, S., Robineau, S., Chardin, P., Paris, S., Chabre, M., Cherfils, J., and Antonny, B. (1998) *The EMBO journal***17**(13), 3651-3659
37. Zhang, B., Zhang, Y., Shacter, E., and Zheng, Y. (2005) *Biochemistry***44**(7), 2566-2576
38. Robineau, S., Chabre, M., and Antonny, B. (2000) *Proceedings of the National Academy of Sciences of the United States of America***97**(18), 9913-9918
39. Peyroche, A., Antonny, B., Robineau, S., Acker, J., Cherfils, J., and Jackson, C. L. (1999) *Molecular cell***3**(3), 275-285
40. Papalia, G., and Myszka, D. *Analytical biochemistry***403**(1-2), 30-35
41. Peyroche, A., Paris, S., and Jackson, C. L. (1996) *Nature***384**(6608), 479-481
42. Mossessova, E., Corpina, R. A., and Goldberg, J. (2003) *Molecular cell***12**(6), 1403-1411
43. Paris, S., Beraud-Dufour, S., Robineau, S., Bigay, J., Antonny, B., Chabre, M., and Chardin, P. (1997) *The Journal of biological chemistry***272**(35), 22221-22226
44. Lenzen, C., Cool, R. H., Prinz, H., Kuhlmann, J., and Wittinghofer, A. (1998) *Biochemistry***37**(20), 7420-7430
45. Smith, W. J., Hamel, B., Yohe, M. E., Sondek, J., Cerione, R. A., and Snyder, J. T. (2005) *Biochemistry***44**(40), 13282-13290
46. Okamura, H., Nishikiori, M., Xiang, H., Ishikawa, M., and Katoh, E. *Structure***19**(7), 988-998
47. Jian, X., Gruschus, J. M., Sztul, E., and Randazzo, P. A. *The Journal of biological chemistry***287**(29), 24273-24283
48. Chang, C. H., Cha, S., Brockman, R. W., and Bennett, L. L., Jr. (1983) *Biochemistry***22**(3), 600-611
49. Stalder, D., Barelli, H., Gautier, R., Macia, E., Jackson, C. L., and Antonny, B. *The Journal of biological chemistry***286**(5), 3873-3883
50. Hafner, M., Schmitz, A., Grune, I., Srivatsan, S. G., Paul, B., Kolanus, W., Quast, T., Kremmer, E., Bauer, I., and Famulok, M. (2006) *Nature***444**(7121), 941-944

51. Saenz, J. B., Sun, W. J., Chang, J. W., Li, J., Bursulaya, B., Gray, N. S., and Haslam, D. B. (2009) *Nature chemical biology***5**(3), 157-165
52. Boal, F., Guetzoyan, L., Sessions, R. B., Zeghouf, M., Spooner, R. A., Lord, J. M., Cherfils, J., Clarkson, G. J., Roberts, L. M., and Stephens, D. J. *Traffic (Copenhagen, Denmark)***11**(12), 1537-1551
53. Ohashi, Y., Iijima, H., Yamaotsu, N., Yamazaki, K., Sato, S., Okamura, M., Sugimoto, K., Dan, S., Hirono, S., and Yamori, T. *The Journal of biological chemistry***287**(6), 3885-3897

Acknowledgements. We thank Sylvie Berger for helpful discussions during SPR data analysis, Corinne Henriquet for experiments performed on CM5 chip, Kadi-Ouahabi Abderrahmane for his technical assistance.

FOOTNOTES: Jad Rouhana is a recipient of a “MENRT” grant from the French government.

Abbreviations.

The abbreviations used are: ARF, ADP-ribosylation factor; Arno, ARF nucleotide-binding site opener; Arno4M, a mutant of Arno carrying four BFA-sensitizing mutations; BFA, Brefeldin A; SPR, Surface Plasmon Resonance; RU, Resonance Unit level; GEF, Guanine Nucleotide Exchange Factors; Bodipy-GTP, guanosine 5'-triphosphate, BODIPY, 2'-(or-3')-O-(N-(2-aminoethyl)urethane).

Figure Legends.

Scheme 1: Simplified model for the binding of Arno Sec7 domain and Mg^{2+} -GDP to separate but interacting sites on Arf1 leading to the formation of a transient Arf1- Mg^{2+} -GDP-Sec7 domain complex, which converts to the binary Arf1-Sec7 domain complex or a pentameric Arf1- Mg^{2+} -GDP-BFA-Sensitive Sec7 domain complex in the presence of BFA. How the pentameric complex dissociates is not perfectly understood so far.

Scheme 2: The GDP to GTP nucleotide exchange on Arf1 upon binding to Sec7 domain.

FIGURE 1: Impact of additional tags on protein activities and sensitivity to BFA. (A) Kinetics of GDP to GTP nucleotide exchange on $[\Delta 17]$ Arf1 (1 μ M) catalyzed by His-AviTags-Arno4M (0,2 μ M) in the presence of Bodipy-GTP (1 μ M) and variable concentrations of BFA (0-200 μ M) as indicated. The nucleotide exchange reaction was initiated with the addition of 1 μ M Bodipy-GTP and monitored by time-resolved fluorescence. AU, arbitrary units. As indicated, by measuring the nucleotide exchange of $[\Delta 17]$ Arf1 using a fluorescent GTP analog, the sensitivity of His-AviTags-Arno4M to BFA was confirmed as the kinetic exchange rate decreases with increasing concentrations of the toxin.

(B) Determination of the apparent inhibition constants (K_{iapp}) of BFA measured with $[\Delta 17]$ Arf1 and either Arno (BFA resistant) or Arno4M (BFA sensitive) with or without additional His-AviTags (HB-Arno4M and HB-Arno). Kinetics measurements were performed in the presence of 1 μ M $[\Delta 17]$ Arf1- Mg^{2+} -GDP, 1 μ M Bodipy-GTP, 0,2 μ M of corresponding GEF Sec7 domain and increasing concentrations of BFA (0-200 μ M).

(C) Analysis of the inhibitory mechanism of BFA on His-AviTags-Arno4M activity using a Michaelis-Menten plot. Kinetics of nucleotide exchange were performed with 50 nM of His-AviTags-Arno4M, 5 μ M Bodipy-GTP, and variable concentrations of $[\Delta 17]$ Arf1- Mg^{2+} -GDP (0-2 μ M) in the presence of BFA (0-100 μ M).

(D) Comparison of nucleotide exchange catalyzed by Arno on $[\Delta 17]$ Arf1 (1 μ M) with or without biotinylated AviTag performed in the presence of 1 μ M of either AviTag- $[\Delta 17]$ Arf1 (B- $[\Delta 17]$ Arf1) or $[\Delta 17]$ Arf1 in the absence or the presence of 0,2 μ M of ARNO as indicated. AU, arbitrary units.

FIGURE 2 : Schematic representation illustrating the strategy on CAP surface with immobilized Sec7 domain. Capture of the biotinylated ligand (Sec7 domain of Arno/Arno4M, purple) on streptavidin conjugated with a ss-DNA oligo (green), subsequent injection of the $[\Delta 17]$ Arf1-Mg²⁺-GDP analyte sample (Arf1, red) followed by dissociation of the Arf1-Arno complex and regeneration of Arno with 2 μ M GDP.

FIGURE 3: Sensorgrams of binding of $[\Delta 17]$ Arf1-Mg²⁺-GDP with Arno determined by SPR. Typical kinetics of $[\Delta 17]$ Arf1- Mg²⁺-GDP binding to immobilized Arno (A) and Arno4M (B) both at 220 RU. Increasing concentrations of Arf1 were injected (50, 100, 200, 400, 800 and 1600 nM, from bottom to top).

Kinetics of $[\Delta 17]$ Arf1-Mg²⁺-GDP binding, with (C) or without (D) a 10 min preincubation of EDTA (10mM), to immobilized Arno (500 RU). Increasing concentrations of Arf1 were injected (6.25, 12.5, 25, 50, 100, 200, from bottom to top).

FIGURE 4: Schematic representation illustrating the strategy on CAP surface with the capture of the biotinylated ligand $[\Delta 17]$ Arf1-GDP (Arf1, red) on the captured streptavidin conjugated with a ss-DNA oligo (green), the saturation with biotin of free streptavidin sites (biotin, blue circle), subsequent injection of the Arno analyte sample (Arno, purple) and complete regeneration of the CAP surface. The Binding of Arno to $[\Delta 17]$ Arf1 is assumed to be concomitant to the release of GDP.

FIGURE 5: Complex formation detection in the presence of GDP or GTP.

- A) Representative sensorgrams of $[\Delta 17]$ Arf1 binding at 200 nM on immobilized Arno or Arno4M with or without 2 μ M of GDP in the injection buffer.
- B) Effect of GDP and GTP concentrations on the binding ratio of $[\Delta 17]$ Arf1 (800 nM) on immobilized Arno (350 RU) measured on the plateau levels at equilibrium in presence of increasing concentrations of nucleotides. The mixture of $[\Delta 17]$ Arf1 with GDP and GTP was performed during injection on the chip. After the last assay with 1 μ M concentration of GDP/GTP, $[\Delta 17]$ Arf1 was flowing again without nucleotide to confirm the overall GEF stability.

FIGURE 6: $[\Delta 17]$ Arf1-Mg²⁺-GDP binding to Arno and Arno4M in the presence of BFA and GDP. Kinetics of $[\Delta 17]$ Arf1-Mg²⁺-GDP binding to immobilized (A) Arno (383 RU) and (B) Arno4M (355 RU) in the presence of 2 μ M GDP and 100 μ M BFA during the association time. Increasing concentrations of Arf1 were injected (25, 50, 100, 200, 400, 800 and 1600 nM, from bottom to top).

FIGURE 7: Kinetics of $[\Delta 17]$ Arf1-Mg²⁺-GDP binding to (A) Arno (383 RU) and (B) Arno4M (665 RU) in the presence of BFA (100 μ M) during the association phase. Increasing concentrations of Arf1 were injected (50, 100, 200, 400, 800 and 1600 nM, from bottom to top). Heterogeneous model components of the fitting curves for Arno4M at three concentrations of Arf1, 1600 nM (panel C), 400 nM (panel D) and

25 nM (panel E). In each, (a) Non-deconvoluted total curve from panel B, (b) AB2 pentameric complex (c) AB1 binary complex and (d) bulk +drift (BiaEvaluation software 4.2).

FIGURE8: Top: Ribbon representation of Arf1 and Arno structures at different steps of the GDP to GTP nucleotide exchange. Arf1 full length or delta-17 truncated bound to Mg^{2+} -GDP (2K5U, 1U81, respectively) and bound to Mg^{2+} -GTP (1O3Y) is in green with Switch 1, InterSwitch and Switch 2 in yellow, red and purple, respectively. Arno in the abortive pentameric complex trapped by BFA (1R8Q) as well as GEA2 in the binary complex (from Golberg, 1998) are colored in dark blue. **Panels A et B** show complex association and dissociation during the two phases in function of conditions used in SPR experiments. Complexes that have been detected are indicated in dark blue.

Tables.

Table 1A: Kinetic Constants of $[Δ17]$ Arf1-Mg²⁺-GDP binding to captured Arno and Arno4M at 25°C, pH 8.0, 150mM NaCl, derived from data displayed in Figure 3, panel A& B. Langmuir1:1 reversible binding model. SR : Stoichiometric ratio

	ka (1/Ms)	kd (1/s)	Rmax (RU)	kd/ka nM	χ^2	SR
Arno	2.19 10 ⁵	4.16 10 ⁻³	45	19	1.37	0.3
Arno4M	2.64 10 ⁵	4.74 10 ⁻³	35	18	1.09	0.27

Table 1B: Kinetic Constants of $[Δ17]$ Arf1-Mg²⁺-GDP binding to captured Arno at different temperatures at pH 8.0 and 150 mM NaCl. Langmuir1:1 reversible binding model. χ^2 value of 0.7 measured for all the curves simultaneously in global-local. SR : Stoichiometric ratio

	ka (1/Ms)	kd (1/s)	Rmax (RU)	kd/ka nM	SR
25°C	2.56 10 ⁵	4.76 10 ⁻³	45	19	0.23
20°C	1.30 10 ⁵	3.30 10 ⁻³	29	25	0.15
15°C	1.20 10 ⁵	2.27 10 ⁻³	23	19	0.12
10°C	9.54 10 ⁴	2.19 10 ⁻³	12	23	0.06

Table 1C: Effect of pH and salt concentrations on Kinetic Constants of $[Δ17]$ Arf1-Mg²⁺-GDP binding to captured Arno at 25°C. Langmuir1:1 reversible binding model. χ^2 value of 0.4 measured for all the curves simultaneously in global-local. SR : Stoichiometric ratio

	ka (1/Ms)	kd (1/s)	Rmax (RU)	kd/ka nM	SR
pH 7, NaCl 150 mM	1.67 10 ⁵	3.81 10 ⁻³	31	23	0.16
pH 8, NaCl 300 mM	1.46 10 ⁵	3.58 10 ⁻³	64	25	0.33

Table 2: Kinetic Constants of $[Δ17]$ Arf1-GDP binding to captured Arno, with or without a 10 min EDTA (10 mM) preincubation of the G protein, derived from data displayed in Figure 3, panel C & D. Langmuir1:1 reversible binding model.

	ka (1/Ms)	kd (1/s)	Rmax (RU)	kd/ka (nM)	χ^2	SR
+EDTA	3.95 10 ⁵	4.19 10 ⁻³	223	10.6	25.5	0.68
- EDTA	1.66 10 ⁵	3.85 10 ⁻³	76	23.2	5.15	0.32

Table 3: Kinetic Constants of [$\Delta 17$]Arf1-GDP binding to captured Arno, at 1 mM and 1 μ M MgCl₂ obtained by kinetic titration experiments (n=3). Langmuir1:1 reversible binding model.

	ka (1/Ms)	kd (1/s)	Rmax (RU)	kd/kanM	χ^2	SR
1 μM	$5.05 \cdot 10^5$	$6.14 \cdot 10^{-3}$	178	12.1	6.4	0.52
1 mM	$2.34 \cdot 10^5$	$5.75 \cdot 10^{-3}$	106	26.5	6.4	0.31

Table 4: Kinetic Constants of Arno binding to captured [$\Delta 17$]Arf1-GDP after 10 min of running buffer containing or not 10mM of EDTA.

Langmuir1:1 reversible binding model						
	ka (1/Ms)	kd (1/s)	Rmax (RU)	kd/kanM	χ^2	SR
- EDTA	$2.66 \cdot 10^4$	$5.54 \cdot 10^{-3}$	220	220	6.37	0.91
Heterogenous ligand binding model						
+ EDTA	ka1 (1/Ms)	kd1 (1/s)	Rmax1 (RU)	kd ₁ /ka ₁ nM	χ^2	SR1
	$1.13 \cdot 10^5$	$5.01 \cdot 10^{-3}$	128	44	23.2	0.46
	ka2 (1/Ms)	kd2 (1/s)	Rmax2 (RU)	kd ₂ /ka ₂ nM		SR2
	$1.67 \cdot 10^4$	$5.65 \cdot 10^{-3}$	152	338		0.54

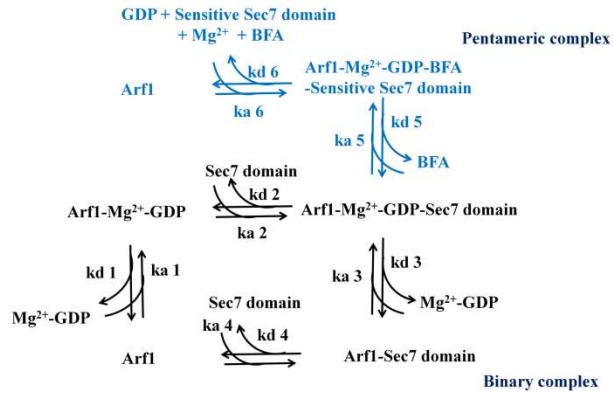
Table 5: Kinetic Constants of [$\Delta 17$]Arf1-Mg²⁺-GDP binding to captured Arno4M and Arno in the presence of 100 μ M BFA with 2 μ M GDP during association phase, derived from data displayed in Figure 6, panel A & B.

	ka (1/Ms)	kd (1/s)	Rmax (RU)	kd/kanM	χ^2	SR
Langmuir1:1 reversible binding model.						
Arno 4M	$6.27 \cdot 10^3$	$3.26 \cdot 10^{-4}$	192	52	0.81	0.79
Heterogenous ligand binding model						
Arno	ka1 (1/Ms)	kd1 (1/s)	Rmax1 (RU)	kd ₁ /ka ₁ nM	χ^2	SR1
	$4.62 \cdot 10^3$	$1.59 \cdot 10^{-3}$	49	344	0.96	0.19
	ka2 (1/Ms)	kd2 (1/s)	Rmax2 (RU)	kd ₂ /ka ₂ nM		SR2
	$3.32 \cdot 10^4$	$3.61 \cdot 10^{-2}$	51	1086		0.19

Table 6: Kinetic Constants of [$\Delta 17$]Arf1-Mg²⁺-GDP binding to captured Arno4M (665 RU) and Arno (383 RU) in the presence of 100 μ M BFA during association phase and without GDP, derived from data displayed in Figure 7, panel A & B.

Heterogenous ligand binding model						
	ka1 (1/Ms)	kd1 (1/s)	Rmax (RU)	kd ₁ /ka ₁ nM	χ^2	SR
Arno 4M	$2.04 \cdot 10^5$	$2.91 \cdot 10^{-3}$	77	14	4.58	0.17
	ka2 (1/Ms)	kd2 (1/s)	Rmax2 (RU)	kd ₂ /ka ₂ nM		SR2
	$3.20 \cdot 10^3$	$0.70 \cdot 10^{-4}$	302	22		0.66
Langmuir1:1 reversible binding model						
	ka (1/Ms)	kd (1/s)	Rmax1 (RU)	kd/kanM	χ^2	SR
Arno	$2.08 \cdot 10^5$	$4.5 \cdot 10^{-3}$	55	22	2.26	0.21

Scheme 1



Scheme2

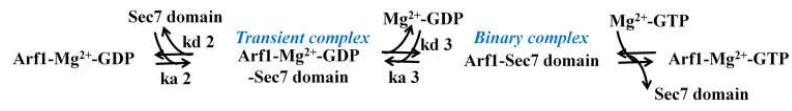


Figure 1

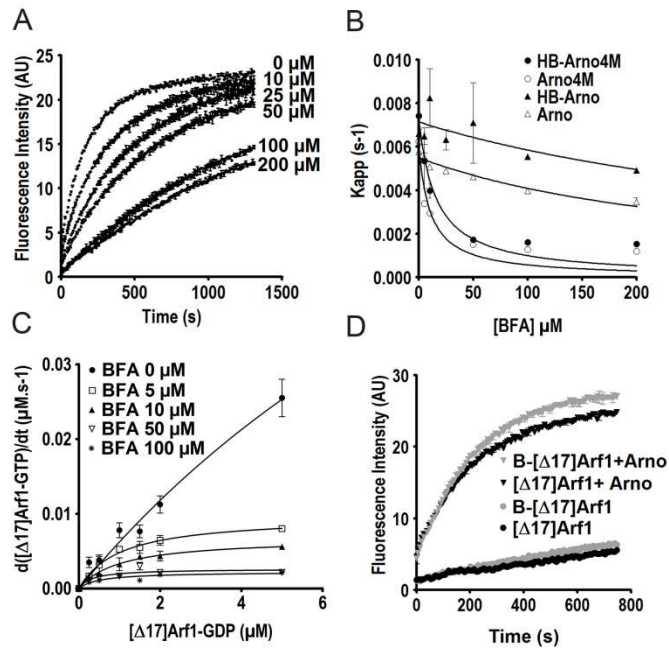


Figure 2.

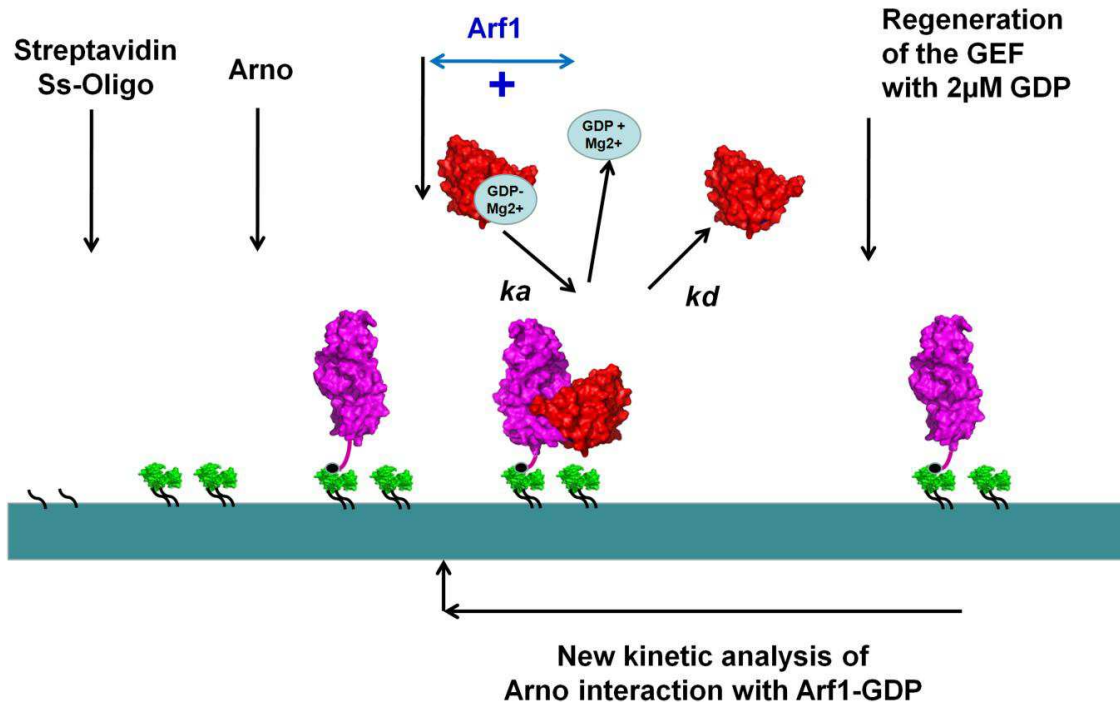


Figure 3.

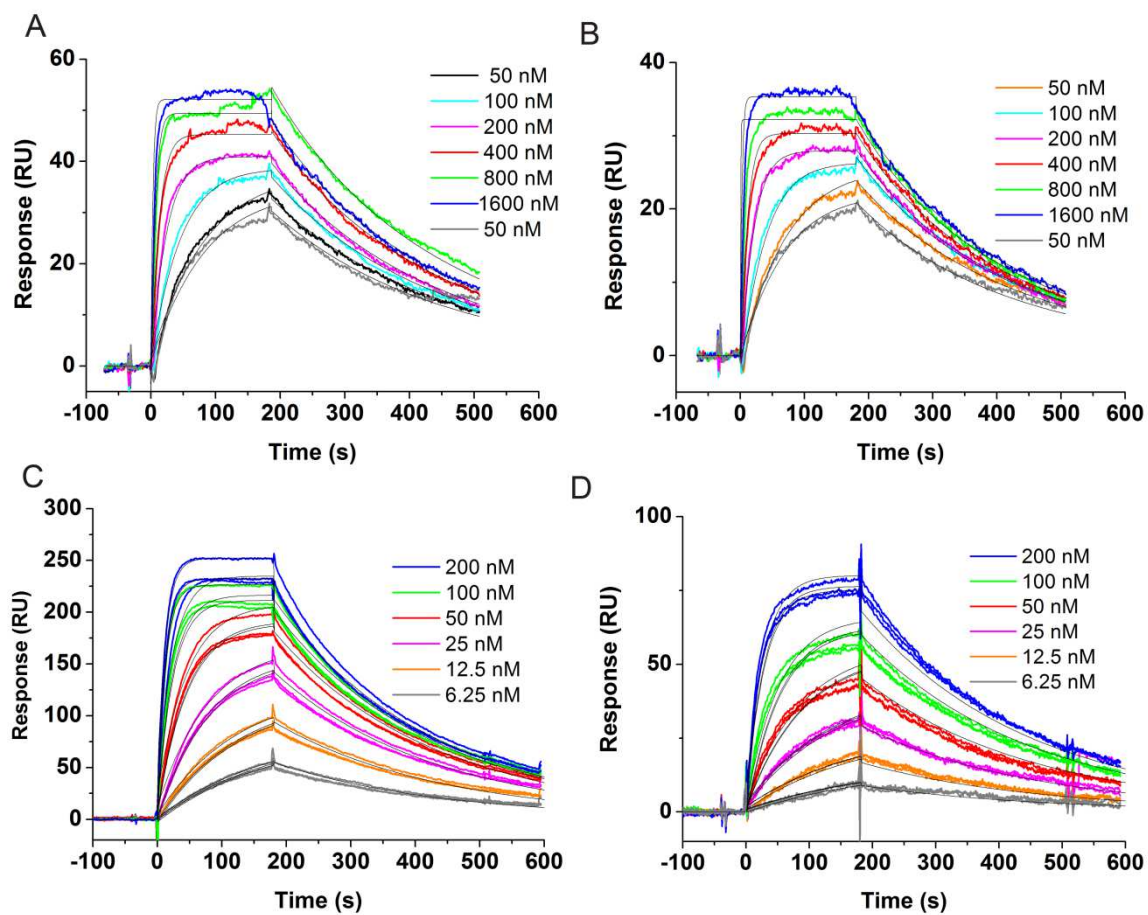


Figure 4

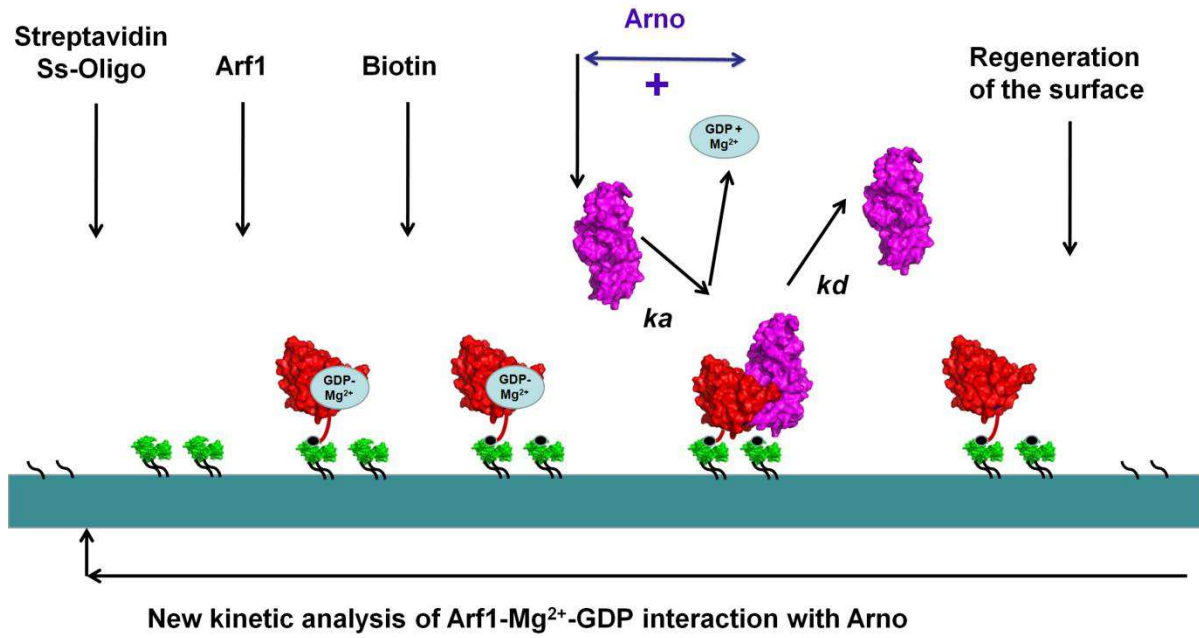


Figure 5

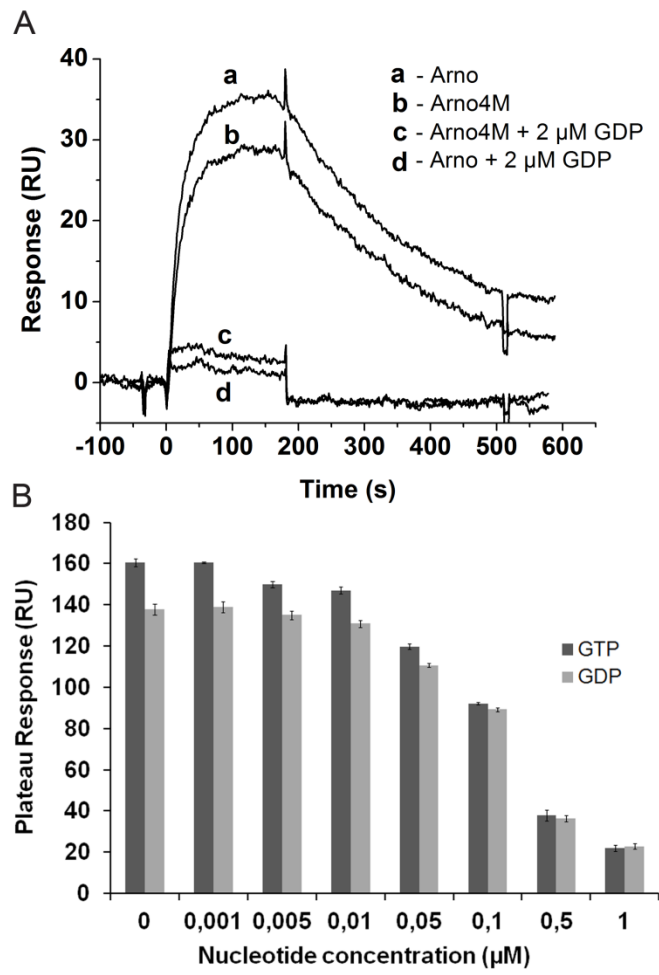


Figure 6

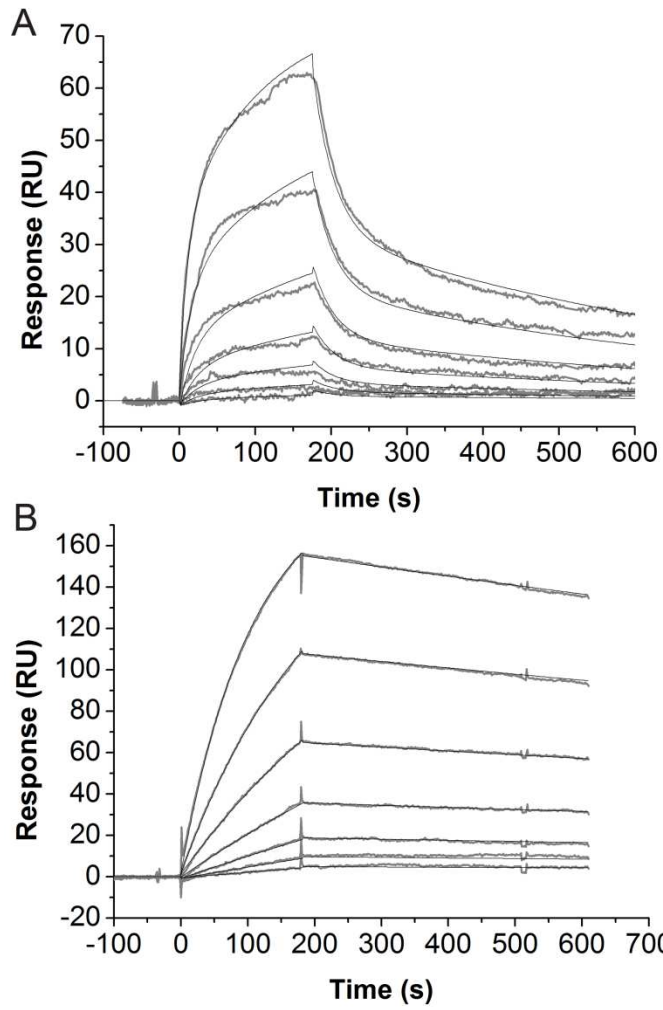


Figure 7

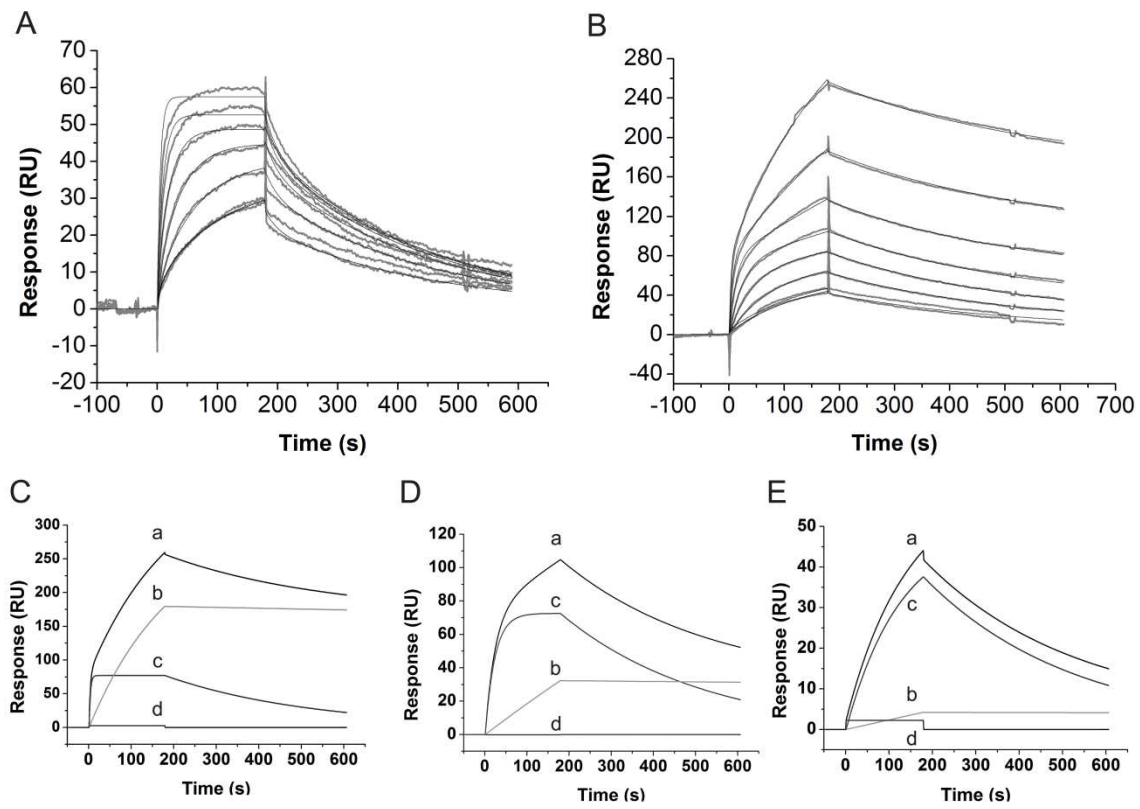


Figure 8